IEEE Access
Multidisciplinary | Rapid Review | Open Access Journal

Received May 10, 2018, accepted June 6, 2018, date of publication June 11, 2018,
date of current version January 16, 2019.

Digital Object Identifier 10.1109/ACCESS.2018.2845904

Adaptive Robust Control of Multi-Axle Vehicle Electro-Hydraulic Power Steering System With Uncertain Tire Steering Resistance Moment

HENG DU, ZHONGBAO WANG, YAXIONG WANG, (Member, IEEE), AND HUI HUANG
School of Mechanical Engineering and Automation, Fuzhou University, Fuzhou 350016, China

Corresponding author: Heng Du (duheng@fzu.edu.cn)

This work was supported in part by the National Natural Science Foundation of China under Grant 51405084, in part by the China Scholarship Council under Grant 201606655019, and in part by the Key Laboratory of Fluid Power and Intelligent Electro-Hydraulic Control, Fuzhou University, Fujian Province, China.

ABSTRACT To investigate the unknown (uncertain) tire steering resistance moment and model uncertainties in a multi-axle vehicle electro-hydraulic power steering system (EHPSS), including the steering mechanisms, valve-controlled double hydraulic actuators, and heavy-duty tires, an adaptive robust control algorithm is developed to estimate the tire steering resistance moment online and compensate for the model uncertainties of EHPSS. The proposed control strategy consists of an adaptive control law and a robust controller which are based on a Lyapunov function. The adaptive control law is employed to update estimated values of the (unknown) tire steering resistance moment and parameter uncertainties in the EHPSS, whereas complicated nonlinearities are addressed by the robust controller. All adaptive laws of the EHPSS and controller, which can impede parametric uncertainties and stabilize the EHPSS, are synthesized by backstepping techniques. The comparative simulation results demonstrate that the proposed adaptive robust control scheme can achieve the desired performance for feasible tracking trajectories despite the existence of an uncertain tire steering resistance moment and external disturbance in the EHPSS.

INDEX TERMS Multi-axle steering, electro-hydraulic servo steering, adaptive control, robust control, motion control.

I. INTRODUCTION

Multi-axle vehicles have been extensively employed in industrial transportation, engineering machinery and other fields, such as heavy cranes, container vehicles and construction machinery [1], [2]. Their market shares have been substantially increased in the large heavy load engineering vehicle industry due to the excellent trafficability and maneuverability of multi-axle vehicles [3]. A multi-axle steering system is one of the most indispensable components of multi-axle vehicle chassis technology. The low-speed flexibility and high-speed stability of vehicle steering motion are substantially dependent on the performance of the multi-axle steering system. A multi-axle steering system has experienced the development of mechanical, hydraulic, electric and electro-hydraulic power steering systems (EHPSSs) [4]. Conventional mechanical, hydraulic, and electric steering systems have completely failed to address the challenges of low-speed flexibility, high-speed stability, and high-frequency overloading [4]. An EHPSS, which consists of a hydraulic power steering system and an electro-hydraulic servo control system, is extensively employed in multi-axle vehicles [5]–[8].

Due to its composite structure, a highly complex nonlinear mathematical model of EHPSS, including the steering mechanisms, valve-controlled double hydraulic actuators with the inherent highly nonlinear dynamics of a hydraulic system and heavy-duty tires [4], causes difficulties in the control of an EHPSS. In addition, the coupling motion relationship among these three parts significantly increases the difficulty of precise control during the turning process. Many efforts are needed to address these obstacles and improve the control performance of an EHPSS.

Previously, a large number of linear control strategies have been applied in multi-axle steering systems. For example, Li *et al.* [9] considered a large-scale transportation vehicle as an example and proposed a cross-coupled control method that is based on system-level contour control in a networked control system. However, a system model must be linearized

in the design of a linear controller, which will close a loss of some important dynamic characteristics of the system [10]. The selection of a nonlinear control method that is suitable for EHPSS is essential.

In recent years, with increasingly stringent steering performance demands in all aspects, such as high-precision tracking, nonlinear behaviors and model uncertainties [11], [12] in an EHPSS, the development of advanced controllers for an EHPSS has encountered significant challenges. In [13] and [14], a state feedback linearization technique has been applied to an electro-hydraulic servo control system; however, this control strategy does not effectively handle the system modeling uncertainties. To address the system modeling uncertainties, a large number of nonlinear control strategies, such as nonlinear robust control [15]–[17], nonlinear adaptive control based on backstepping techniques [19], [20], and control methods based on a nonlinear disturbance observer, have been designed [21]. Yao *et al.* [12] and Bu and Yao [22] successfully applied adaptive robust control based on backstepping techniques to an electro-hydraulic servo control system, which not only adresses the parameter uncertainties but also compensates for the unmodeled dynamics.

Some novel nonlinear adaptive control strategies [23]–[25], [30] have been successfully applied to an electro-hydraulic servo control system. These strategies not only solve the control challenges that originate from nonlinear systems under certain conditions but also demonstrate that nonlinear control schemes are superior to traditional linear controllers in precise-tracking, parametric uncertainties, and nonlinear disturbance attenuation [10]. However, research and pertinent data on nonlinear control of an EHPSS, which includes a hydraulic power steering system and an electro-hydraulic servo control system, are rare.

Note that the performance of single-axle steering has a decisive role in a multi-axle steering system and is significant for the precise tracking of a single-axle steering system. In this paper, based on the research in [4], an adaptive robust controller that is based on a Lyapunov function and a controlled parameter update law while utilizing backstepping techniques to synthesize the entire single-axle steering system controller and parameter adaptive laws, are designed. To test the performance of the proposed controller, several comparative simulation results are provided for a uniaxial EHPSS.

This paper is organized as follows: a nonlinear dynamic model of a uniaxial EHPSS are presented in Section II. In Section III, an adaptive robust controller design process and an analysis of stability theories are discussed. Comparative simulation results are presented in Section IV. In Section V, conclusions are discussed.

II. NONLINEAR DYNAMIC MODEL OF UNIAXIAL EHPSS

The three-dimensional structure of a uniaxial EHPSS is shown in Fig. 1. This EHPSS can be decomposed into two subsystems: (a) a mechanical steering system that consists of steering wheels and a trapezoid mechanism; (b) a hydraulic power drive steering system that comprises two actuation cylinders and a servo solenoid valve (shown in Fig. 2) [4].

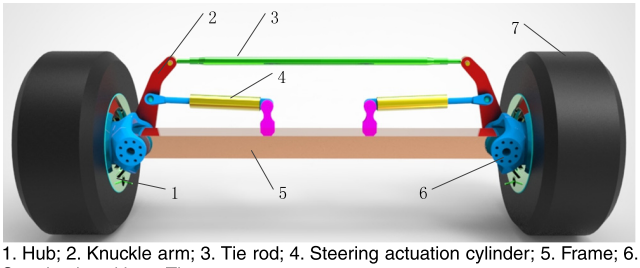

1. Hub; 2. Knuckle arm; 3. Tie rod; 4. Steering actuation cylinder; 5. Frame; 6. Steering knuckle; 7. Tire.

FIGURE 1. Steering mechanisms of uniaxial EHPSS.

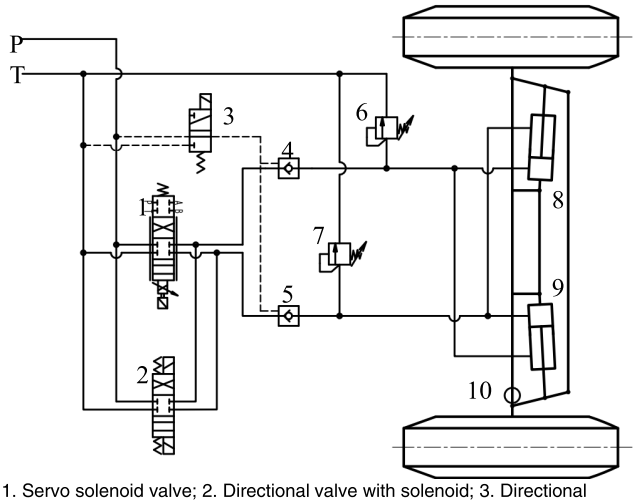

1. Servo solenoid valve; 2. Directional valve with solenoid; 3. Directional poppet valve with solenoid; 4 & 5. Pilot operated check valve; 6 & 7. Relief valve; 8 & 9. Steering actuation cylinders; 10. Angle sensor.

FIGURE 2. Hydraulic system of uniaxial EHPSS.

The hydraulic system of an EHPSS is depicted in Fig. 2. The system includes servo steering, a hydraulic lock, emergency manual operation and overload protection. Brief descriptions are provided in the following section, whereas detailed descriptions are described in [3].

Servo Steering: As shown in Fig. 2, hydraulic actuators 8 and 9 are controlled by valve 1. Other valves are in a normal position. **Hydraulic lock:** The wheels can be locked in their required positions in steering mode; In this case, valves 1 and 3 are powered-off, and valves 4 and 5 are open; then, the hydraulic actuators can be locked; **Emergency manual operation:** If valve 1 is out of control, valve 2 can be used to move the wheels to the left or right by manual operation; **Overload protection:** Relief valves 6 and 7 are used as safety valves to protect hydraulic actuators 8 and 9 from high-pressure impact [4].

A. KINEMATIC AND DYNAMIC MODELING OF THE STEERING MECHANISMS

As shown in Fig. 3, the rotation angle of the right tire around the main pin is β, the rotation angle of the left tire around the main pin is α and the relationship between the rotation angle of the left tire and the rotation angle of the right tire can be described as

$$\begin{cases} \alpha = \arccos\dfrac{k^2+m^2-L^2}{2km} + \arcsin\dfrac{m\sin(\gamma-\beta)}{k} - \gamma \\ k = \sqrt{B^2+m^2-2Bm\cos(\gamma-\beta)} \end{cases} \tag{1}$$

where γ is the intersection angle between the steering knuckle arm and the beam of the axle at the midpoint, B is the distance between two kingpins in a single axle, L is the tie rod length, and m is the steering knuckle arm length [4].

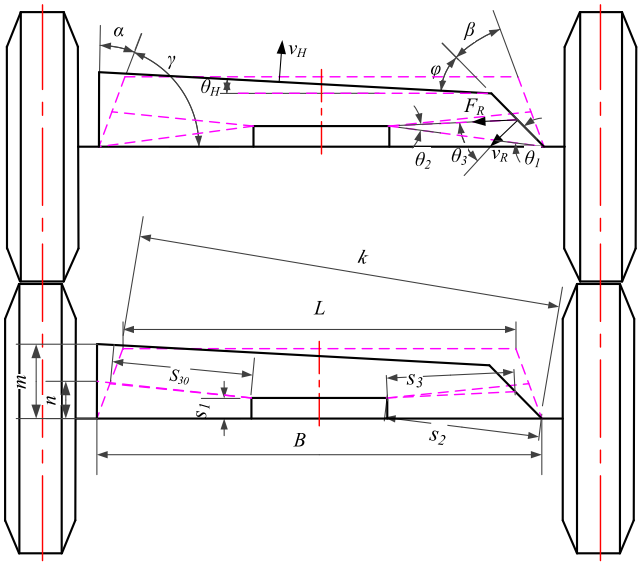

FIGURE 3. Dynamics analysis diagram of the steering mechanisms.

If the gap between the steering mechanisms is not considered, the degree of freedom of the EHPSS can be calculated as $DOF = 7 \times 3\text{-}2 \times 10 = 1$. Steering system mechanisms motions are divided into three groups: 1. Rotation of the left tire, wheel hub, and steering knuckle arm around the left master pin, with an equivalent moment of inertia J_L; 2. Rotation of the right tire, wheel hub, and steering knuckle arm around the right master pin, with an equivalent moment of inertia J_R; 3. Tie rod movement, which can be regarded as planar and divided into translation and rotation around its centroid [4].

Elastic deformation occurs when a small steering angle is generated and U manifests as elastic potential energy of the tires, but an analytic model for tire elastic characteristics is somewhat difficult to construct. As a result, U is regarded as an external load in this paper. The kinetic energy of the tie rods is substantially less than the kinetic energy of the tire steering part, which has minimal influence on the kinetic energy of the entire steering system. Therefore, the kinetic energy of the tie rods can be disregarded without affecting the performance of the system. The total kinetic energy and dissipative energy of the system are expressed as

$$\begin{aligned} T &= \frac{1}{2}J_L\dot{\alpha}^2 + \frac{1}{2}J_R\dot{\beta}^2 \\ D &= \frac{1}{2}C_L\dot{\alpha}^2 + \frac{1}{2}C_R\dot{\beta}^2 \end{aligned} \tag{2}$$

where C_L are the equivalent damping coefficients of the left tire and the equivalent damping coefficients of the right tire is C_R [4]. The Lagrange equation satisfied by the EHPSS can be expressed as

$$\frac{\mathrm{d}}{\mathrm{d}t}\left(\frac{\partial T}{\partial\dot{\beta}}\right) - \frac{\partial T}{\partial\beta} + \frac{\partial D}{\partial\dot{\beta}} = Q \tag{3}$$

where Q represents the generalized force, and according to the virtual velocity method, Q can be obtained

$$Q = \frac{F_R v_R\cos\theta_3 + F_L v_L\cos\theta_3' - T_L\dot{\alpha} - T_R\dot{\beta}}{\dot{\beta}} \tag{4}$$

where v_L is the left hydraulic actuator's velocity, and v_R is the right hydraulic actuator's velocity; F_L is the hydraulic driving force of the left hydraulic actuator and F_R is the hydraulic driving force of the right hydraulic actuator; T_L is the left tire resistance moment, and T_R is the right tire resistance moment [4]. As shown in Fig. 1, the angle θ_3 between F_R and v_R and the angle θ_3' between F_L and v_L can be described as

$$\begin{aligned} v_L &= \dot{\alpha}n \\ v_R &= \dot{\beta}n \\ \theta_3 &= \frac{\pi}{2} - \theta_1 - \theta_2 \\ \theta_1 &= \gamma - \beta - \arcsin(s_1/s_2) \\ s_3 &= \sqrt{n^2+s_2^2-2ns_2\cos\theta_1} \end{aligned} \tag{5}$$

$$\theta_2 = \arccos\frac{s_3^2+s_2^2-n^2}{2s_2s_3} \tag{6}$$

$$\begin{aligned} \theta_3' &= -\frac{\pi}{2} + \theta_1' + \theta_2' \\ \theta_1' &= \gamma + \alpha - \arcsin(s_1/s_2) \\ s_3' &= \sqrt{n^2+s_2^2-2ns_2\cos\theta_1'} \end{aligned}$$

$$\theta_2' = \arccos\frac{s_3'^2+s_2^2-n^2}{2s_2s_3'} \tag{7}$$

$$\begin{aligned} x_R &= s_{30} - s_3 \\ x_L &= s_3' - s_{30} \end{aligned} \tag{8}$$

where definitions of all geometric parameters in (5)-(8) are provided in the Appendix of [4]. Substituting (2) and (4) into (3), the dynamic equation of all steering mechanisms can be expressed as

$$\begin{aligned} M_1\ddot{\beta} = {} & n\cos\theta_3 F_R + n\cos\theta_3' F_L(b_1+b_2) - T_L(b_1+b_2) \\ & - T_R - M_2\dot{\beta}^2 - M_3\dot{\beta} - f(\beta,\dot{\beta},t) \end{aligned} \tag{9}$$

where

$$c_1 = \frac{k^2 + m^2 - L^2}{2km}, \quad c_2 = \frac{m\sin(\gamma - \beta)}{k}$$
$$b_1 = -\frac{1}{\sqrt{1 - c_1^2}}\frac{\partial c_1}{\partial \beta}, \quad b_2 = \frac{1}{\sqrt{1 - c_2^2}}\frac{\partial c_2}{\partial \beta}$$
$$M_1 = J_L(b_1 + b_2)^2 + J_R$$
$$M_2 = J_L(b_1 + b_2)(\frac{\partial b_1}{\partial \beta} + \frac{\partial b_2}{\partial \beta})$$
$$M_3 = C_L(b_1 + b_2)^2 + C_R \tag{10}$$

In (10), $f(\beta, \dot{\beta}, t)$ represents uncertain nonlinearities, including unmodeled dynamics and external disturbance.

B. MODELING OF HYDRAULIC SYSTEM

The hydraulic system of the EHPSS in this paper is shown in Fig. 4.

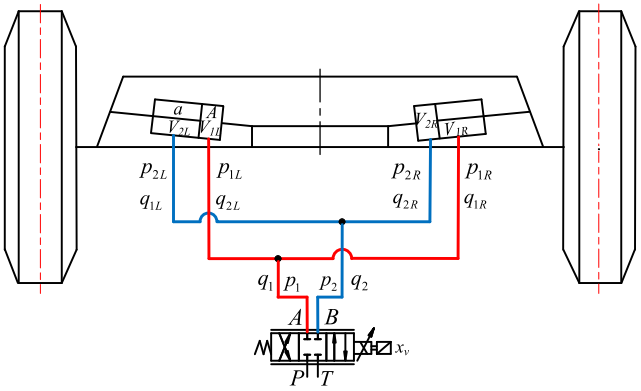

FIGURE 4. The hydraulic system of EHPSS.

As depicted in Fig. 4, q_1 is the total flow into and q_2 is the total flow out of the two steering actuation cylinders. q_1 and q_2 are related to the spool valve displacement of the servo solenoid valve x_v by [26]

$$q_1 = \sqrt{2}k_{q1}x_v[s(x_v)\sqrt{(p_s - p_1)} + s(-x_v)\sqrt{(p_1 - p_r)}]$$
$$q_2 = \sqrt{2}k_{q2}x_v[s(x_v)\sqrt{(p_2 - p_r)} + s(-x_v)\sqrt{(p_s - p_2)}] \tag{11}$$

where

$$k_{q1} = C_d w_1\sqrt{\frac{1}{\rho}}, k_{q2} = C_d w_2\sqrt{\frac{1}{\rho}} \tag{12}$$

and defining function s(•) [10] as

$$s(\bullet) = \begin{cases} 1 & if \bullet \geq 0 \\ 0 & if \bullet < 0 \end{cases} \tag{13}$$

where p_1 and p_2 are the working pressure of port A and port B, respectively. C_d is the discharge coefficient of the servo-valve; w_1 and w_2 are area gradients of the spool valve; ρ is the hydraulic oil density; p_s is the supply pressure; and p_r is the tank pressure.

The left and right two tires are characterized by high mass and large inertia, which causes the system to be in a low frequency bandwidth of no more than 30 Hz. Furthermore, a high-response servo-valve is used here and the frequency of the valve is higher than 100 Hz in general conditions. Therefore, the frequency of the servo valve is considerably higher than the system bandwidth and the servo valve dynamics can be simplified as a proportion linker. Then the following equation is given by $x_v = k_i u$, where k_i is a positive constant, u is the input voltage.

Assumption 1: The servo valve is matched and symmetrical, that is, $k_{q1} = k_{q2} = k_q$. p_1 and p_2 are both bounded by $0 < p_r < p_1 < p_s$, $0 < p_r < p_2 < p_s$ under normal working conditions.

Basing on Assumption 1, we can obtain

$$q_1 = gR_1 u$$
$$q_2 = gR_2 u \tag{14}$$

where g $= k_q k_i$ and

$$R_1 = s(u)\sqrt{(p_s - p_1)} + s(-u)\sqrt{(p_1 - p_r)}$$
$$R_2 = s(u)\sqrt{(p_2 - p_r)} + s(-u)\sqrt{(p_s - p_2)} \tag{15}$$

To simplify the analysis, some feasible engineering assumptions are proposed.

Assumption 2: 1. Hydraulic energy is an ideal constant pressure source, that is, the supply pressure p_s is constant, and the tank pressure p_r is zero. 2. The line between a servo solenoid valve and an actuation cylinder is short, that is, its length has a negligible effect on the system [10].

Based on Assumption 2, we can obtain

$$q_1 = q_{1L} + q_{1R}$$
$$q_2 = q_{2L} + q_{2R}$$
$$p_1 = p_{1L} = p_{1R}$$
$$p_2 = p_{2L} = p_{2R} \tag{16}$$

where q_{1L} and q_{2L} are the supplied flow and the return flow, respectively, of the left cylinder; q_{1R} and q_{2R} are the supplied flow and the return flow of the right cylinder respectively; p_{1L} and p_{2L} are the pressures in two chambers of the left cylinder, and p_{1R} and p_{2R} are the pressures in two chambers of the right cylinder [10].

The hydraulic cylinders dynamics can be based on [26], and the left hydraulic cylinder dynamics can be expressed as

$$a\dot{x}_L + C_{ip}(p_{1L} - p_{2L}) - C_{ep}p_{2L} - q_{2L} = V_{2L}\dot{p}_{2L}/\beta_e$$
$$A\dot{x}_R + C_{ip}(p_{1R} - p_{2R}) - C_{ep}p_{2R} - q_{2R} = V_{2R}\dot{p}_{2R}/\beta_e \tag{17}$$

Similarly, the right hydraulic cylinder dynamics can be expressed as

$$q_{1L} - A\dot{x}_L - C_{ip}(p_{1L} - p_{2L}) - C_{ep}p_{1L} = V_{1L}\dot{p}_{1L}/\beta_e$$
$$q_{1R} - a\dot{x}_R - C_{ip}(p_{1R} - p_{2R}) - C_{ep}p_{1R} = V_{1R}\dot{p}_{1R}/\beta_e \tag{18}$$

In (17) and (18), C_{ip} is the internal leakage coefficient, C_{ep} is the external leakage coefficient; x_L and x_R are the left cylinder displacement and the right cylinder displacement, respectively; A and a are areas of the two hydraulic chambers;

V_{1L} and V_{2L} are volumes of the left cylinder two chambers; and V_{1R} and V_{2R} are volumes of the right cylinder two chambers [4].

According to (16), (17) and (18), we can obtain

$$\begin{aligned} q_1 &= A\dot{x}_L + a\dot{x}_R + 2C_{ip}(p_1 - p_2) + 2C_{ep}p_1 \\ &\quad + (V_t/2 + Ax_L + ax_R)\dot{p}_1/\beta_e \\ q_2 &= a\dot{x}_L + A\dot{x}_R + 2C_{ip}(p_1 - p_2) - 2C_{ep}p_2 \\ &\quad - (V_t/2 - ax_L - Ax_R)\dot{p}_2/\beta_e \end{aligned} \tag{19}$$

and

$$\begin{aligned} V_{1L} &= V_{1L0} + Ax_L \\ V_{1R} &= V_{1R0} + ax_R \\ V_{2L} &= V_{2L0} - ax_L \\ V_{2R} &= V_{2R0} - Ax_R \\ V_t &= 2(V_{1L0} + V_{1R0}) = 2(V_{2L0} + V_{2R0}) \end{aligned} \tag{20}$$

where V_{1L0} and V_{2L0} are the initial volumes of the left cylinder two chambers; V_{2R0} and V_{1R0} are the initial volumes of the right cylinder two chambers; and V_t is the total volume of each cylinder [4].

Define the state variables of EHPSS as $x = [x_1, x_2, x_3, x_4]^{\mathrm{T}} = [\beta, \dot{\beta}, p_1, p_2]^{\mathrm{T}}$ and disregard external leakages. Combining (9), (14) and (19), the state space equation of EHPSS can be expressed as

$$\begin{aligned} \dot{x}_1 &= x_2 \\ M_1\dot{x}_2 &= n\cos\theta_3 F_R + n\cos\theta_3' F_L(b_1 + b_2) - T_L(b_1 + b_2) \\ &\quad - T_R - M_2x_2^2 - M_3x_2 - d(x_1, x_2, t) \\ \dot{x}_3 &= \frac{\beta_e}{V_t/2 + Ax_L + ax_R}[-A\frac{\partial x_L}{\partial x_1}x_2 - a\frac{\partial x_R}{\partial x_1}x_2 \\ &\quad - 2C_{ip}(x_3 - x_4) + gR_1u] \\ \dot{x}_4 &= \frac{\beta_e}{V_t/2 - ax_L - Ax_R}[a\frac{\partial x_L}{\partial x_1}x_2 + A\frac{\partial x_R}{\partial x_1}x_2 \\ &\quad + 2C_{ip}(x_3 - x_4) - gR_2u] \end{aligned} \tag{21}$$

where

$$\begin{aligned} F_L &= p_1A - p_2a \\ F_R &= p_1a - p_2A \end{aligned} \tag{22}$$

Given the desired trajectory $x_d(t)$, the main purpose of this paper is to design a bounded control input u, which can guarantee the output $y = x_1$ tracks $x_d(t)$ as accurately as possible. In an actual hydraulic system, the following assumptions are given.

Assumption 3: The ideal tracking trajectory $x_d(t)$ and its speed $\dot{x}_d(t)$ and acceleration $\ddot{x}_d(t)$ are bounded.

III. NONLINEAR ADAPTIVE ROBUST CONTROLLER DESIGN

A. DESIGN MODEL AND ISSUES TO BE ADDRESSED

The parametric uncertainties have to be considered due to changes in $T_L, T_R, C_L, C_R, C_{ip}$, and C_{ep} during the steering motion. The mathematical model of the system is quite complex, which increases the complexity of the resulting control law. For simplicity, we only consider uncertain parameters that have a greater impact on the performance of the system, such as T_L, T_R, C_{ip} and the nominal value (i.e., d_n) of the lumped unmodeled dynamics d [22]. To use the adaptive law to address parametric uncertainties, the system state space equation should be linearly parameterized. Therefore, we can define the unknown parameter set $\varphi = [\varphi_1, \varphi_2, \varphi_3, \varphi_4]^{\mathrm{T}} = [T_L, T_R, d_n, C_{ip}]^{\mathrm{T}}$. To ensure that the subsequent nonlinear controller design is concise and easy to read, the system equation (21) is replaced by some symbolic variables. Then, the system equation is transformed as

$$\begin{aligned} \dot{x}_1 &= x_2 \\ \dot{x}_2 &= \frac{1}{M_1}[F - \varphi_1(b_1 + b_2) - \varphi_2 - M_2x_2^2 - M_3x_2] \\ &\quad - \varphi_3 - \tilde{d}(x_1, x_2, t) \\ \dot{x}_3 &= -f_1 - \varphi_4 f_2 + f_3u \\ \dot{x}_4 &= f_4 + \varphi_4 f_5 - f_6u \end{aligned} \tag{23}$$

where

$$\begin{aligned} F &= n\cos\theta_3 F_R + n\cos\theta_3' F_L(b_1 + b_2) \\ \tilde{d}(x_1, x_2, t) &= \frac{1}{M_1}f(x_1, x_2, t) - d_n \\ f_1 &= \frac{\beta_e}{V_t/2 + Ax_L + ax_R}(A\frac{\partial x_L}{\partial x_1}x_2 + a\frac{\partial x_R}{\partial x_1}x_2) \\ f_2 &= \frac{2\beta_e}{V_t/2 + Ax_L + ax_R}(x_3 - x_4) \\ f_3 &= \frac{\beta_e gR_1}{V_t/2 + Ax_L + ax_R} \\ f_4 &= \frac{\beta_e}{V_t/2 - ax_L - Ax_R}(a\frac{\partial x_L}{\partial x_1}x_2 + A\frac{\partial x_R}{\partial x_1}x_2) \\ f_5 &= \frac{2\beta_e}{V_t/2 - ax_L - Ax_R}(x_3 - x_4) \\ f_6 &= \frac{\beta_e gR_2}{V_t/2 - ax_L - Ax_R} \end{aligned} \tag{24}$$

Although the true values of these unknown parameters are unknown, the approximate range of these parameters can be obtained in (23) based on the following assumptions.

Assumption 4: The boundaries of the unknown parameter set φ and uncertain nonlinearities $\tilde{d}$ are obtained

$$\begin{aligned} \varphi \subset \Omega_\varphi &\triangleq \{\varphi : \varphi_{\min} \le \varphi \le \varphi_{\max}\} \\ \left|\tilde{d}(x_1, x_2, t)\right| &\le D \end{aligned} \tag{25}$$

where $\varphi_{\min} = [\varphi_{1\min}, \varphi_{2\min}, \varphi_{3\min}, \varphi_{4\min}]^{\mathrm{T}}$, $\varphi_{\max} = [\varphi_{1\max}, \varphi_{2\max}, \varphi_{3\max}, \varphi_{4\max}]^{\mathrm{T}}$, and D are known.

B. DISCONTINUOUS PROJECTION MAPPING

Let $\tilde{\varphi}$ represent the estimated value of φ and $\tilde{\varphi}$ represent the estimation error (i.e., $\tilde{\varphi} = \hat{\varphi} - \varphi$). The following

discontinuous projection mapping can be obtained by [12]

$$\mathrm{Proj}_{\hat{\varphi}}(\bullet_i) = \begin{cases} 0 & \text{if } \hat{\varphi}_i = \varphi_{i\max} \text{ and } \bullet_i > 0 \\ 0 & \text{if } \hat{\varphi}_i = \varphi_{i\min} \text{ and } \bullet_i < 0 \\ \bullet_i & \text{otherwise} \end{cases} \tag{26}$$

In (26), $i = 1, 2, 3,$ and 4 and $\bullet_i$ represents the i-th element in the vector $\bullet$. Then, a controlled adaptive law can be expressed as

$$\dot{\hat{\varphi}} = \mathrm{Proj}_{\hat{\varphi}}(\Gamma\tau) \tag{27}$$

where Γ is a positive definite adaptive rate diagonal matrix, and τ represents an adaptive function that is subsequently synthesized. In addition, the discontinuous projection mapping employed in (27) satisfies

$$\begin{aligned} &(P_1)\ \hat{\varphi} \subset \Omega_{\hat{\varphi}} \triangleq \{\hat{\varphi} : \varphi_{\min} \le \varphi \le \varphi_{\max}\} \\ &(P_2)\ \tilde{\varphi}^T[\Gamma^{-1}\mathrm{Proj}_{\hat{\varphi}}(\Gamma\tau) - \tau] \le 0, \quad \forall\tau \end{aligned} \tag{28}$$

C. DESIGN CONTROLLER

The recursive backstepping design method is utilized to design an adaptive robust controller because system equation (23) includes the mismatched model uncertainties.

Step 1: Note that no uncertainties exist in the first equation of (23), and a simple ARC Lyapunov function can be directly constructed for the first two equations (23) [22]. A switching-function-like quantity is defined as

$$z_2 = \dot{z}_1 + k_1 z_1 = x_2 - x_{2eq}, x_{2eq} = \dot{x}_d - k_1 z_1 \tag{29}$$

where $z_1 = x_1 - x_d(t)$ characterizes the tracking error of the system, and k_1 is a positive feedback gain. The Laplace transformation of the first equation (29) is $z_1(s) = G(s)z_2(s)$, and $G(s) = 1/(s+k_1)$ is a stable transfer function. Therefore, if z_2 converges to zero or a small value, then z_1 will converge to zero or a small value. The objective is to obtain the smallest value for z_2 in the next design.

Combining (23) and (29), $\dot{z}_2$ can be expressed as

$$\begin{aligned} \dot{z}_2 &= \dot{x}_2 - \dot{x}_{2eq} \\ &= \frac{1}{M_1}F - \frac{1}{M_1}[\varphi_1(b_1+b_2) + \varphi_2 + M_2x_2^2 + M_3x_2] \\ &\quad - \varphi_3 - \tilde{d}(x_1, x_2, t) - \dot{x}_{2eq} \end{aligned} \tag{30}$$

In (30), $\dot{x}_{2eq} = \ddot{x}_d - k_1\dot{z}_1$ is computable. If F/M_1 is regarded as the virtual control input of (30), we will be able to structure a virtual control function α_2 for F/M_1 to guarantee that z_2 is as small as possible. The ARC approach proposed in [12] by be employed to make z_2 as small as possible by eliminating both parametric uncertainties (i.e., $\varphi_1, \varphi_2, \varphi_3$) and the uncertain nonlinearity $\tilde{d}$. The virtual control function α_2 can be constructed as

$$\begin{aligned} \alpha_2(x_1, x_2, \hat{\theta}_1, \hat{\theta}_2, t) &= \alpha_{2a} + \alpha_{2s} \\ \alpha_{2a} &= \frac{1}{M_1}[\hat{\varphi}_1(b_1+b_2) + \hat{\varphi}_2 + M_2x_2^2 + M_3x_2] \\ &\quad + \hat{\varphi}_3 + \dot{x}_{2eq} \\ \alpha_{2s} &= \alpha_{2s1} + \alpha_{2s2}, \quad \alpha_{2s1} = -k_{2s1}z_2 \end{aligned} \tag{31}$$

where k_{2s1} is a positive nonlinear control gain, by designing appropriate k_{2s1} and k_1 to render the matrix Λ_2 defined in (32) positive.

$$\Lambda_2 = \begin{bmatrix} k_1^3 & -\frac{1}{2}k_1^3 \\ -\frac{1}{2}k_1^3 & k_{2s1} \end{bmatrix} \tag{32}$$

From (31), α_2 consists of two parts—α_{2a} and α_{2s}—and α_{2a} is employed to improve the model compensation by utilizing the parameter adaption law given in (27) to update the estimated values of unknown parameters in real time, which is equivalent to an adaptive controller based on the system model. α_{2s} contains two parts α_{2s1} and α_{2s2}, where α_{2s1} can be considered as a stable linear feedback of the system and α_{2s2} is a robust controller to be structured.

Let $z_3 = F/M_1 - \alpha_2$ represent the D-value between F/M_1 and α_2; substituting (31) into (30), $\dot{z}_2$ can be obtained as

$$\dot{z}_2 = z_3 - k_{2s1}z_2 + \alpha_{2s2} - \phi_2^{\mathrm{T}}\tilde{\varphi} - \tilde{d}(x_1, x_2, t) \tag{33}$$

where $\phi_2 = [-\frac{b_1+b_2}{M_1}, -\frac{1}{M_1}, -1, 0]^{\mathrm{T}}$.

The robust controller α_{2s2} is selected to guarantee the following inequations [12]

$$\begin{aligned} &(1)\ z_2[\alpha_{2s2} - \phi_2^{\mathrm{T}}\tilde{\varphi} - \tilde{d}(x_1, x_2, t)] \le \varepsilon_2 \\ &(2)\ z_2\alpha_{2s2} \le 0 \end{aligned} \tag{34}$$

In (34), $\varepsilon_2 > 0$ is a controller design parameter that is given an arbitrarily small value. From the first inequation of (34), α_{2s2} is employed to dominate the model uncertainties due to the parametric uncertainties $\tilde{\varphi}$ and uncertain nonlinearities $\tilde{d}$. The other inequation of (34) guarantees that α_{2s2} is dissipating in nature because it cripples the coupling between α_{2s2} and α_{2a} [12]. The selection method of α_{2s2} that satisfied (34) is described in **Lemma 5**.

Defining a positive semi-definite Lyapunov function as

$$V_2 = \frac{1}{2}z_2^2 + \frac{1}{2}k_1^2z_1^2 \tag{35}$$

By combining (29) and (33), the time derivative of V_2 can be obtained

$$\begin{aligned} \dot{V}_2 = z_2z_3 - k_{2s1}z_2^2 + k_1^2z_1z_2 - k_1^3z_1^2 \\ + z_2[\alpha_{2s2} - \phi_2^{\mathrm{T}}\tilde{\varphi} - \tilde{d}(x_1, x_2, t)] \end{aligned} \tag{36}$$

from (34)

$$\dot{V}_2 \le z_2z_3 - k_{2s1}z_2^2 + k_1^2z_1z_2 - k_1^3z_1^2 + \varepsilon_2 \tag{37}$$

Step 2: From (37), if F/M_1 can accurately track α_2, i.e., $z_3 = 0$, the tracking error z_1, z_2 of the system will be bounded and enter into a set area over time. Thus, the objective is to make z_3 converge to zero with a guaranteed transient performance in the next design.

Combining the system state space equation (23) and the definition of z_3, $\dot{z}_3$ can be obtained as

$$\dot{z}_3 = \frac{M_1\dot{F} - \dot{M}_1F}{M_1^2} - \dot{\alpha}_2 \tag{38}$$

where

$$\dot{F} = d_1 - \varphi_4(h_2 + h_5) + (h_3 + h_6)u \tag{39}$$

Substituting (39) into (38), $\dot{z}_3$ can be transformed as

$$\dot{z}_3 = \frac{(h_3 + h_6)}{M_1}u - \phi_4\frac{(h_2 + h_5)}{M_1} + \frac{d_1}{M_1} - \frac{\dot{M}_1 F}{M_1^2} - \dot{\alpha}_2 \tag{40}$$

In (39) and (40)

$$\begin{aligned} d_1 = &-n\sin\theta_3\frac{\partial\theta_3}{\partial x_1}x_2F_R + n[-\sin\theta_3'\frac{\partial\theta_3'}{\partial x_1}x_2(b_1 + b_2) \\ &+ \cos\theta_3'(\frac{\partial b_1}{\partial x_1}x_2 + \frac{\partial b_2}{\partial x_1}x_2)]F_L - h_1 - h_4 \end{aligned} \tag{41}$$

$$\begin{aligned} h_1 &= n\cos\theta_3(af_1 + Af_4) \\ h_2 &= n\cos\theta_3(af_2 + Af_5) \\ h_3 &= n\cos\theta_3(af_3 + Af_6) \\ h_4 &= n\cos\theta_3'(Af_1 + af_4) \\ h_5 &= n\cos\theta_3'(Af_2 + af_5) \\ h_6 &= n\cos\theta_3'(Af_3 + af_6) \end{aligned} \tag{42}$$

$$\tag{43}$$

In (40), $\dot{\alpha}_2$ consists of two parts; its expression is

$$\dot{\alpha}_2 = \dot{\alpha}_{2c} + \dot{\alpha}_{2u} \tag{44}$$

where

$$\begin{aligned} \dot{\alpha}_{2c} &= \frac{\partial\alpha_2}{\partial t} + \frac{\partial\alpha_2}{\partial x_1}x_2 + \frac{\partial\alpha_2}{\partial x_2}\hat{\dot{x}}_2 + \frac{\partial\alpha_2}{\partial\hat{\varphi}}\dot{\hat{\varphi}} \\ \dot{\alpha}_{2u} &= \frac{\partial\alpha_2}{\partial x_2}\tilde{\dot{x}}_2 \end{aligned} \tag{45}$$

$$\begin{aligned} \hat{\dot{x}}_2 &= \frac{1}{M_1}[F - \hat{\varphi}_1(b_1 + b_2) - \hat{\varphi}_2 - M_2x_2^2 - M_3x_2] - \hat{\varphi}_3 \\ \tilde{\dot{x}}_2 &= \tilde{\varphi} - \tilde{d}(x_1, x_2, t) \end{aligned} \tag{46}$$

where $\dot{\alpha}_{2c}$ employed in the design of the final controller denotes a calculable partial differential part in $\dot{\alpha}_2$. However, $\dot{\alpha}_{2u}$ cannot have the same denotation due to the inclusion of unknown uncertainties, which need to be dominated by robust feedback.

Based on (40) and (44)-(46), the final adaptive robust controller can be synthesized with the following structure

$$\begin{aligned} u &= u_a + u_s \\ u_a &= \frac{M_1}{h_3 + h_6}(-\frac{d_1}{M_1} + \hat{\varphi}_4\frac{h_2 + h_5}{M_1} + \frac{\dot{M}_1 F}{M_1^2} + \dot{\alpha}_{2c}) \\ u_s &= \frac{M_1}{h_3 + h_6}(u_{s1} + u_{s2}) \\ u_{s1} &= -k_{3s1}z_3 \end{aligned} \tag{47}$$

where k_{s31} is a positive nonlinear control gain, by designing appropriate k_{2s1}, k_{s31} and k_1 to render the matrix Λ_3 defined in (48) positive.

$$\Lambda_3 = \begin{bmatrix} k_1^3 & -\frac{1}{2}k_1^3 & 0 \\ -\frac{1}{2}k_1^3 & k_{2s1} & -\frac{1}{2} \\ 0 & -\frac{1}{2} & k_{2s1} \end{bmatrix} \tag{48}$$

From (48), α_2 consists of parts u_a and u_s, and u_a is employed to improve the model compensation by utilizing the parameter adaption law given in (27) to update the estimated values of unknown parameters in real time, which is equivalent to an adaptive controller based on the system model. u_s contains two parts—u_{s1} and u_{s2}, and u_{s1} can be considered to be a stable linear feedback of the system, and u_{s2} is a robust controller to be structured.

Substituting (47) into (40), $\dot{z}_3$ can be transformed as

$$\dot{z}_3 = -k_{3s1}z_3 + u_{s2} - \varphi_3^{\mathrm{T}}\tilde{\varphi} + \frac{\partial\alpha_2}{\partial x_2}\tilde{d}(x_1, x_2, t) \tag{49}$$

where

$$\phi_3^{\mathrm{T}} = [\frac{\partial\alpha_2}{\partial x_2}\frac{b_1 + b_2}{M_1}, \frac{\partial\alpha_2}{\partial x_2}\frac{1}{M_1}, \frac{\partial\alpha_2}{\partial x_2}, -\frac{M_1}{h_1 + h_2}] \tag{50}$$

The robust controller u_{s2} is selected to guarantee the following inequations

$$\begin{aligned} &(1)\ z_3[u_{s2} - \phi_3^{\mathrm{T}}\tilde{\varphi} + \frac{\partial\alpha_2}{\partial x_2}\tilde{d}(x_1, x_2, t)] \le \varepsilon_3 \\ &(2)\ z_3u_{s2} \le 0 \end{aligned} \tag{51}$$

In (34), $\varepsilon_3 > 0$ is a controller design parameter given an arbitrarily small value. The selection method of u_{s2} that satisfied (51) is described in Lemma 5.

D. MAIN RESULTS

Choosing the adaptive function $\tau = \phi_2 z_2 + \phi_3 z_3$, the estimation value of the unknown system parameters can be updated in real time by the parameter adaptive law (27). Based on the design process of the entire adaptive robust controller, the adaptive robust control strategy synthesized in this paper has the following properties [12], [22].

A.

All signals involved in the closed-loop controller are bounded. Then, we define the following Lyapunov function:

$$V_3 = V_2 + \frac{1}{2}z_3^2 \tag{52}$$

and V_3 has to satisfy the following condition

$$V_3 \le \exp(-\mu_V t)V_3(0) + \frac{\varepsilon_V}{\mu_V}[1 - \exp(-\mu_V t)] \tag{53}$$

where $\mu_V = 2\lambda_{\min}(\Lambda_3)\ \min\{1/k_1^2, 1, 1\}$, $\varepsilon_V = \varepsilon_2 + \varepsilon_3$, and $\lambda_{\min}(\Lambda_3)$ denote the minimum eigenvalue of the positive definite matrix Λ_3.

B.

After the finite time t_s, if only parameter uncertainties exist in the system, that is, $\tilde{d} = 0$, we obtain not only the conclusion in A but also an adaptive robust controller (47) that can guarantee the gradual tracking performance of the system, that is, $z \to 0$ as $t \to \infty$, where $z = [z_1, z_2, z_3]^{\mathrm{T}}$.

Proof: Please refer to Appendix.

IV. COMPARATIVE SIMULATIONS

A. CONTROLLER SIMPLIFICATION

From the theoretical results, we can select the appropriate robust feedback terms according to conditions (34) and (51). Then, the following chosen lemma α_{2s2} and u_{s2} can be given using similar results in [12].

Lemma 5: Let h_2 be an arbitrary constant that satisfies

$$h_2 \geq \|\phi_2\|^2 \|\varphi_M\|^2 + D^2, \quad \varphi_M = \varphi_{\max} - \varphi_{\min} \tag{54}$$

then, α_{2s2} can be chosen as

$$\alpha_{2s2} = -k_{2s2}(x_1, x_2, \varphi_M, D)z_2 = -\frac{h_2}{2\varepsilon_2}z_2 \tag{55}$$

where k_{2s2} is a nonlinear feedback gain, and α_{2s2} of (55) satisfies (34).

Let h_3 be an arbitrary constant that satisfies

$$h_3 \geq \|\phi_3\|^2 \|\varphi_M\|^2 + (\frac{\partial \alpha_2}{\partial x_2}D)^2, \quad \varphi_M = \varphi_{\max} - \varphi_{\min} \tag{56}$$

then, u_{s2} can be chosen as

$$u_{s2} = -k_{3s2}(x_1, x_2, \varphi_M, D)z_3 = -\frac{h_3}{2\varepsilon_3}z_3 \tag{57}$$

where k_{3s2} is a nonlinear feedback gain, u_{s2} of (57) satisfies (51). The proof of Lemma 5 is presented in Appendix.

Lemma 5 gives the design examples that strictly satisfy (34) and (51). From the point of view of their implementation, the norms of ϕ_2 and ϕ_3 need to be calculated in real time, which produces a more complex implementation of the controller. Another simple method is to make the parameters k_{2s1} and k_{3s1} sufficiently large without considering the specific values of h_2, ε_2 and h_3, ε_3. Although the strictness of (34) and (51) is destroyed, the stability of the system also changes from global stability to local stability while simplifying the realization of the controller. According to the analysis, the simple method of selecting the parameters is not sufficiently rigorous but is simple and effective.

B. PARAMETER SETTING

The system parameters are set as shown in the following table.

TABLE 1. System parameter setting.

symbol	value	unit	symbol	value	unit
A	0.0038	m^2	ρ	870	kg/m^3
a	0.0029	m^2	C_{ip}	4×10^{-12}	$m^3/(s\cdot Pa)$
J_L	143.1	$kg\cdot m^2$	C_d	0.62	\
J_R	143.1	$kg\cdot m^2$	w	0.0364	m
n	0.21	m	V_t	0.002	m^3
β_e	7×10^8	Pa	γ	76	°
B	2.0596	m	m	0.36	m
L	1.8854	m	C_R	4×10^3	N/rad
C_L	4×10^3	N/rad	s_{30}	0.6548	m
p_s	170	bar	s_1	0.17	m
p_r	0	bar	s_2	0.7250	m

C. SIMULATION RESULTS

The effectiveness of the controller proposed in this paper is verified by comparing the tracking performance of the four controllers.

$$y = f(x) + g(x)u + d(t) \tag{58}$$

1) **ARC:** the adaptive robust controller designed in this paper and introduced in Section III.C. According to the controller simplification in Section IV.A, the design parameters of the controller are selected as follows: $k_1 = 260, k_2 = k_{2s1} + k_{2s2} = 208$, and $k_3 = k_{3s1} + k_{3s2} = 130$. From TABLE 1, the initial value of the unknown parameter set φ is selected as: $\hat{\varphi}(0) = [100, 80, 0.5, 4 \times 10^{-12}]^{\mathrm{T}}$, the adaptive rate diagonal matrix is chosen as: $\Gamma = diag[10^{0.5}, 10^{0.6}, 5 \times 10^{-6}, 1.5 \times 10^{-25}]^{\mathrm{T}}$, the bounds of φ are given as: $\varphi_{\min} = [-2500, 2500, 80, 10^{-12}]^{\mathrm{T}}$, $\varphi_{\min} = [2500, 2500, 80, 10^{-11}]^{\mathrm{T}}$.
2) **DRC:**the deterministic robust control scheme. The design process of this controller is the same as the design process of ARC; however, a parameter adaptive law, i.e., $\Gamma = diag[0,0,0,0]^{\mathrm{T}}$, does not exist.
3) **SMC:**the sliding mode control law. Based on the design principle of the sliding mode controller, we have to obtain the third derivative of the system output to obtain the relative order of the system as follows:
Combining (58), the sliding model controller can be designed as

$$u = \frac{1}{g(x)}[-f(x) - (c_1\dot{z}_1 + c_2\ddot{z}_1) + x_d - \eta sgn(s)] \tag{59}$$

where $s = c_1z_1 + c_2\dot{z}_1 + \ddot{z}_1$ denotes the sliding mode surface, and c_1, c_2 and η are positive constants.

As shown in Fig. 2, valve 1 controls two actuation cylinders 8 and 9. Other valves are in the normal position. The wheels can be locked at their required positions in steering mode when the valve 1 and 3 are power-off, and the valve 4 and 5 are open. If valve 1 is out of control, valve 2 can be used to move the wheels left or right by manual operation. Relief valves 6 and 7 are used as safety valves to protect two actuation cylinders 8 and 9 from high pressure impact.

To test the tracking performance of the three controllers, the desired tracking trajectory is a sine curve, i.e., $x_d = 20\sin(t)°$ and its unit is degrees. First, in the case of zero load, i.e., $T_L = 0$, and $T_R = 0$, the tracking errors curve of the three controllers is shown in Fig. 5. As shown in Fig. 5, the three controllers have very small tracking errors in the case of zero load, which confirms the satisfactory performance of the proposed controller. Compared with the tracking errors of DRC and SMC, the tracking error of ARC is the smallest error, which demonstrates the validity of the adaptive law.

The dynamic model of the tires is complexand - establishing an accurate model is difficult. Wang *et al.* [27] established an empirical formula of an in situ resistance

moment and tested the resistance moment of the left and right tires under different loads. The relationship between the return moment and the steering angle is given [28], [29]. Therefore, a simplified model of the tires is established based on these references, as shown in TABLE 2 to TABLE 4.

TABLE 2. Parameters of tire's resistance moment.

Parameters	T_R	T_L
c	2000-100k	600-100k
d	1200-100k	1000-100k
h	600-100k	1500-100k
j	1000-100k	2000-100k
k	0,1,2,…,n	0,1,2,…,n

TABLE 3. Parameters of tire's resistance moment.

Parameters	Value
a	18
b	20
g	15
e	$\frac{ac+bh}{c+h}$
f	$\frac{(j-h)g}{b+a}-\frac{h+j}{2}-\frac{(j-h)(a-b)}{2(a+b)}$
n	$\frac{aj+bd}{d+j}$
m	$-\frac{g(c-d)}{b+a}+\frac{c+d}{2}-\frac{(c-d)(b-a)}{2(b+a)}$

TABLE 4. Value of tire's resistance moment.

Condition	Resistance moment
$t<1.425s$	$\sqrt{\frac{\beta}{5}[\frac{5(c-d)}{b+a}+\frac{(c+d)}{2}-\frac{(c-d)(b-a)}{2(b+a)}]^2}$
$\dot{\beta}>0$ *and* $\beta\geq -g$	$\frac{\beta(c-d)}{b+a}+\frac{(c+d)}{2}-\frac{(c-d)(b-a)}{2(b+a)}$
$\dot{\beta}>0$ *and* $-n<\beta<-g$	$m-\frac{m(\beta+g)^2}{(n-g)^2}$
$\dot{\beta}>0$ *and* $\beta\leq -n$	$\frac{\beta(d+j)}{b-a}+\frac{(d-j)}{2}+\frac{(d+j)(a+b)}{(b-a)}$
$\dot{\beta}<0$ *and* $\beta\geq e$	$\frac{\beta(c+h)}{b-a}+\frac{(c-h)}{2}-\frac{(c+h)(a+b)}{2(b-a)}$
$\dot{\beta}<0$ *and* $g\leq\beta<e$	$f-\frac{f(\beta-g)^2}{(e-g)^2}$
$\dot{\beta}<0$ *and* $\beta<g$	$\frac{\beta(j-h)}{b+a}-\frac{(h+j)}{2}-\frac{(j-h)(a-b)}{2(a+b)}$
$\dot{\beta}=0$ *and* $\beta>0$	$sign(\beta)\cdot c$
else	$sign(\beta)\cdot d$

Then, the model can describe the basic characteristics of the tires [4]. The value of the moment depends on the parameters c, d, h, j, and k. When $k = 0$, the relationship between the tire's resistance moment and the steering angle is shown in Fig. 6.

To test the influence of the uncertain tire steering resistance moment on the performance of the EHPSS, the tire steering resistance moment is added to the closed loop simulation model. The two desired trajectories with different frequencies are given to analyze the performance of the EHPSS at different speeds. A slower sine curve $x_d = 20\sin(0.5t)°$ is given in the case of the position curve of ARC, as shown in Fig. 7, and the very small tracking errors of three controllers are shown in Fig. 8. The error of ARC is minimal. A regular control input is shown in Fig. 9. The tire steering resistance moment has a dominant role in the model uncertainties of the EHPSS at low speed, according to Fig. 7, Fig. 8 and Fig. 9. The proposed

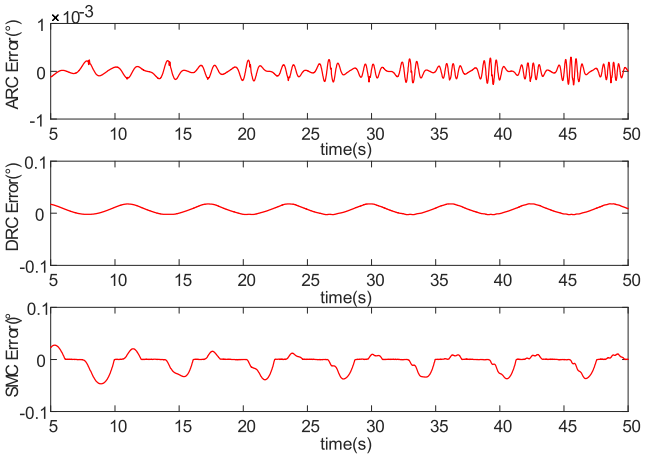

FIGURE 5. Tracking errors of ARC, DRC and SMC without loads.

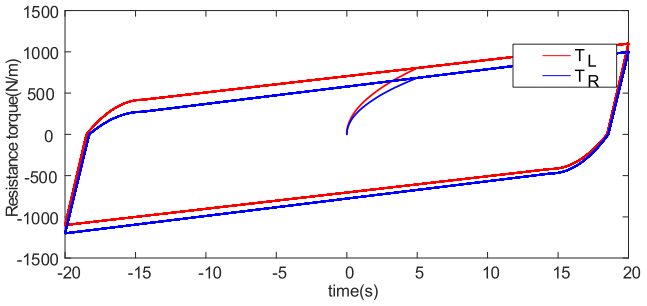

FIGURE 6. Relationship between the tires resistance moment and the steering angle.

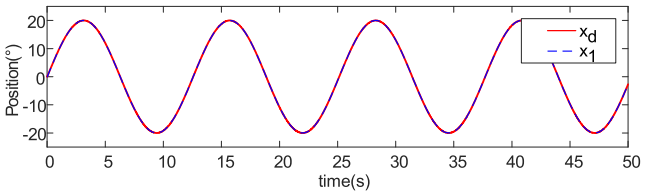

FIGURE 7. Position curve of ARC in slower sine curve with loads.

controller can guarantee a robust performance with the tire steering resistance moment.

Next, the simulation is run for tracking a faster sine curve $x_d = 20\sin(t)°$. The perfect tracking curve and regular control input of ARC are shown in Fig. 10 and Fig. 11 respectively; the errors of three controllers are shown in Fig. 12, in which ARC can achieve better performance than the other two algorithms because ARC compensates for the uncertain tire steering resistance moment and updates constant unknown parameters by the adaption laws presented in Fig. 13. The simulation results indicate that the feasibility and effectiveness of the ARC algorithm proposed in this paper is fully confirmed.

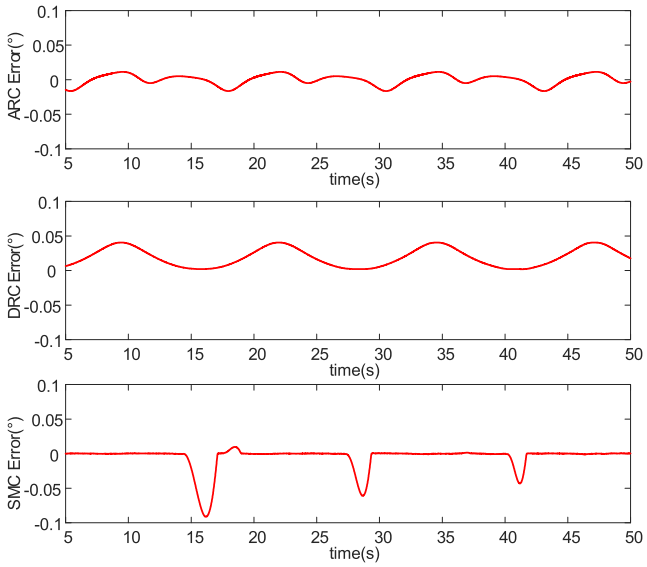

FIGURE 8. Tracking errors of three controllers in slower sine curve with loads.

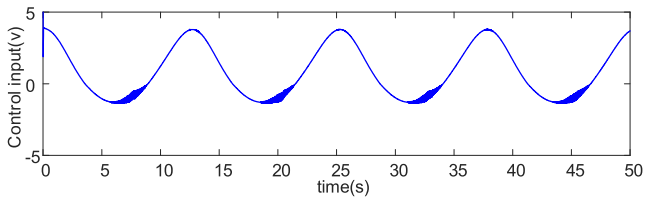

FIGURE 9. Control input of ARC in slower sine curve with loads.

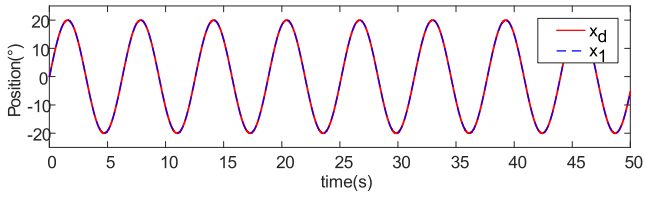

FIGURE 10. Tracking curve of ARC in faster sine curve with loads.

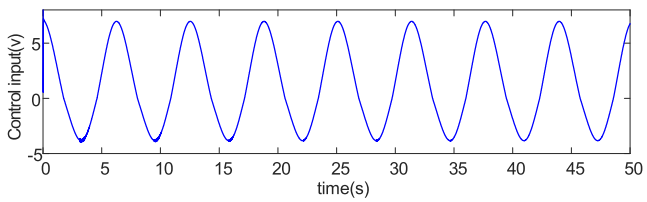

FIGURE 11. Control input of ARC in faster sine curve with loads.

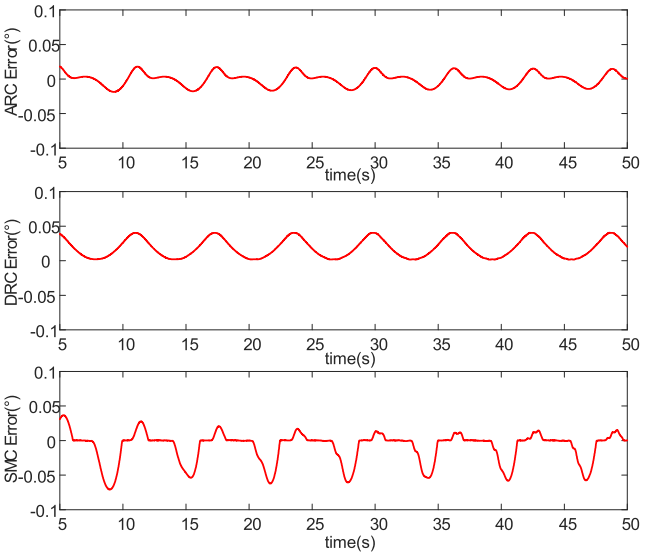

FIGURE 12. Tracking errors of three controllers in faster sine curve with loads.

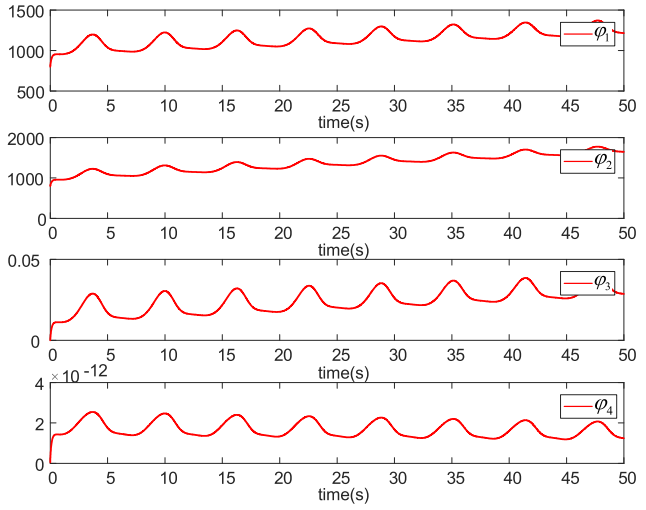

FIGURE 13. Parameter estimation of ARC in faster sine curve with loads.

V. CONCLUSION

In this paper, an adaptive robust control algorithm is synthesized to estimate the uncertain tire steering resistance moment online and compensate for the model uncertainties for a multi-axle vehicle electro-hydraulic power steering system (EHPSS), including steering mechanisms, valve-controlled double hydraulic actuators and heavy-duty tires. This control scheme considers the particular nonlinearities in an EHPSS, such as the steering mechanisms' nonlinearities, the complex nonlinear dynamics in valve-controlled double hydraulic

actuators, the nonlinear dynamics of tires and the coupling motion among these three parts. A MATLAB simulation system is established to realize the precise tracking motion simulation of EHPSS. Extensive comparative simulation results are also given to further verify the effectiveness and excellent performance of the proposed algorithm. The advanced nonlinear control algorithm has been successfully applied to the highly complex multi-axle vehicle steering system, which is a breakthrough and serves as a reference in the nonlinear control of a multi-axle steering system.

APPENDIX A
PROOF OF CONCLUSION A:

From (33) and (49), the time derivative of V_3 can be expressed as

$$\begin{aligned}\dot{V}_3 &= \dot{V}_2 + z_3\dot{z}_3 \\ &= z_2 z_3 - k_{2s1}z_2^2 + k_1^2 z_1 z_2 - k_1^3 z_1^2 \\ &\quad + z_2[\alpha_{2s2} - \phi_2^{\mathrm{T}}\tilde{\varphi} - \tilde{d}(x_1, x_2, t)] \\ &\quad + z_3[-k_{3s1}z_3 + u_{s2} - \phi_3^{\mathrm{T}}\tilde{\varphi} + \frac{\partial \alpha_2}{\partial x_2}\tilde{d}(x_1, x_2, t)] \quad (60)\end{aligned}$$

Note that (34) and (51)

$$\dot{V}_3 \le z_2 z_3 - k_{2s1}z_2^2 + k_1^2 z_1 z_2 - k_1^3 z_1^2 - k_{3s1}z_3^2 + \varepsilon_V \quad (61)$$

According to the matrix (48)

$$\begin{aligned}\dot{V}_3 &\le z^{\mathrm{T}}\Lambda_3 z + \varepsilon_V \le -\lambda_{\min}(\Lambda_3)(z_1^2 + z_2^2 + z_3^2) + \varepsilon_V \\ &\le \varepsilon_V - \mu_V V_3 \quad (62)\end{aligned}$$

in which $z = [z_1, z_2, z_3]^{\mathrm{T}}$, from the principle of contrast

$$V_3 \le \exp(-\mu_V t)V_3(0) + \frac{\varepsilon_V}{\mu_V}[1 - \exp(-\mu_V t)] \quad (63)$$

From (63), V_3 is globally bounded, z_1, z_2, and z_3 are bounded, and the entire signals involved in the controller presented in this paper are bounded.

APPENDIX B
PROOF OF CONCLUSION B:

When the system has only parameter uncertainties, i.e., $\tilde{d} = 0$, the following Lyapunov function is defined as

$$V = V_3 + \frac{1}{2}\tilde{\varphi}^{\mathrm{T}}\Gamma^{-1}\tilde{\varphi} \quad (64)$$

Combining (27) and (62), the time derivative of V is expressed as

$$\begin{aligned}\dot{V} &= z_2 z_3 - k_{2s1}z_2^2 + k_1^2 z_1 z_2 - k_1^3 z_1^2 \\ &\quad + z_2[\alpha_{2s2} - \phi_2^{\mathrm{T}}\tilde{\varphi} - \tilde{d}(x_1, x_2, t)] - k_{3s1}z_3^2 \\ &\quad + z_3[u_{s2} - \phi_3^{\mathrm{T}}\tilde{\varphi} + \frac{\partial \alpha_2}{\partial x_2}\tilde{d}(x_1, x_2, t)] + \tilde{\varphi}^{\mathrm{T}}\Gamma^{-1}\dot{\hat{\varphi}} \quad (65)\end{aligned}$$

Noting (34) and (51)

$$\begin{aligned}\dot{V} \le{}& z_2 z_3 - k_{2s1}z_2^2 + k_1^2 z_1 z_2 - k_1^3 z_1^2 \\ &- k_{3s1}z_3^2 + \tilde{\varphi}^{\mathrm{T}}[-\phi_3 z_2 - \phi_3 z_3 + \Gamma^{-1}\dot{\hat{\varphi}}] \quad (66)\end{aligned}$$

Considering adaptive law (27)

$$\begin{aligned}\dot{V} \le{}& z_2 z_3 - k_{2s1}z_2^2 + k_1^2 z_1 z_2 - k_1^3 z_1^2 - k_{3s1}z_3^2 \\ &+ \tilde{\varphi}^{\mathrm{T}}[\Gamma^{-1}\,\mathrm{Pr}\,oj_{\hat{\varphi}}(\Gamma\tau) - \tau] \quad (67)\end{aligned}$$

considering the second condition in (28)

$$\begin{aligned}\dot{V} &\le z_2 z_3 - k_{2s1}z_2^2 + k_1^2 z_1 z_2 - k_1^3 z_1^2 - k_{3s1}z_3^2 \\ &\le -\lambda_{\min}(\Lambda_3)(z_1^2 + z_2^2 + z_3^2) = -W \quad (68)\end{aligned}$$

In (68), $W \in L_2$, $\dot{W} \in L_\infty$ can be achieved by (29), (33) and (51), i.e., W is uniform continuity. Thus, $W \to 0$ as $t \to \infty$, which leads to **Conclusion B** according to Barbalat's lemma.

The Proof of Lemma 5: From (54), we can obtain $h_2 > 0$; thus, (55) satisfies the first condition of (34). Next, we prove that (55) also xondition of (34) by substituting (55) into the second condition of (34)

$$\begin{aligned}z_2[-\frac{h_2}{2\varepsilon_2}z_2 - \phi_2^{\mathrm{T}}\tilde{\varphi} - \tilde{d}(x_1, x_2, t)] \le{}& -\frac{1}{2}\frac{\|\varphi_2\|^2\,\|\varphi_M\|^2\,z_2^2}{\sqrt{\varepsilon_2}} \\ &- \|\phi_2\|\,\|\varphi_M\|\,|z_2| - \frac{1}{2}\frac{\|D\|^2\,z_2^2}{\sqrt{\varepsilon_2}} - \|D\|\,|z_2| \quad (69)\end{aligned}$$

From Young's inequation, we can prove that (55) also satisfies the second condition of (34); similarly, (57) also satisfies (51).

REFERENCES

[1] A. Aoki, Y. Marumo, and I. Kageyama, "Directional response of multi-articulated vehicles with multiple axles to steering input," *J. Mech. Syst. Transp. Logistics*, vol. 4, no. 2, pp. 79–94, 2011.

[2] J. Zhao, Z. Wang, and Y. Qin, "Simulation and experimental analysis of electro-hydraulic steering control system for TLC900 transporting girder vehicle," *Chin. J. Mech. Eng.*, vol. 43, no. 9, pp. 65–69, Sep. 2007.

[3] H. Du, J. Wei, and J. Fang, "The design, simulation, and experiment of high-accuracy multi-axle electro-hydraulic control servo steering system," *Adv. Mech. Eng.*, vol. 8, no. 10, pp. 1–15, Sep. 2016.

[4] H. Du, Q. Zhang, S. Chen, and J. Fang, "Modeling, simulation, and experimental validation of electro-hydraulic power steering system in multi-axle vehicles," *Proc. Inst. Mech. Eng. D, J. Automobile Eng.*, to be published, doi: 10.1177/0954407017743346.

[5] S. H. Kim, M. C. Shin, and C. N. Chu, "Development of EHPS motor speed map using HILS system," *IEEE Trans. Veh. Technol.*, vol. 62, no. 4, pp. 1553–1567, May 2013.

[6] D. Graovac, B. Koppl, M. Scheffer, M. Purschel, and A. Kiep, "Optimal PWM method for electric and electro-hydraulic power steering applications," in *Proc. IEEE PESC*, Jun. 2008, pp. 3213–3219.

[7] J. Gessat, "Electrically powered hydraulic steering systems for light commercial vehicles," SAE Tech. Paper 2007-01-4197, 2007.

[8] A. Badawy, D. Fehlings, A. Wiertz, and J. Gessat, "Development of a new concept of electrically powered hydraulic steering," SAE Tech. Paper 2004-01-2070, 2004.

[9] Y. Li, L. Yang, and G. Yang, "Network-based coordinated motion control of large-scale transportation vehicles," *IEEE/ASME Trans. Mechatronics*, vol. 12, no. 2, pp. 208–215, Apr. 2007.

[10] C. Guan and S. Pan, "Nonlinear adaptive robust control of single-rod electro-hydraulic actuator with unknown nonlinear parameters," *IEEE Trans. Control Syst. Technol.*, vol. 16, no. 3, pp. 434–445, May 2008.

[11] J. Yao, Z. Jiao, D. Ma, and L. Yan, "High-accuracy tracking control of hydraulic rotary actuators with modeling uncertainties," *IEEE/ASME Trans. Mechatronics*, vol. 19, no. 2, pp. 633–641, Apr. 2014.

[12] B. Yao, F. Bu, J. Reedy, and G. T.-C. Chiu, "Adaptive robust motion control of single-rod hydraulic actuators: Theory and experiments," *IEEE/ASME Trans. Mechatronics*, vol. 5, no. 1, pp. 79–91, Mar. 2000.

[13] R. Vossoughi and M. Donath, "Dynamic feedback linearization for electrohydraulically actuated control systems," *ASME J. Dynam. Syst., Meas., Control*, vol. 117, no. 4, pp. 468–477, 1995.

[14] L. D. Re and A. Isidori, "Performance enhancement of nonlinear drives by feedback linearization of linear-bilinear cascade models," *IEEE Trans. Control Syst. Technol.*, vol. 3, no. 3, pp. 299–308, Sep. 1995.
[15] Z. Chen, B. Yao, and Q. Wang, "Accurate motion control of linear motors with adaptive robust compensation of nonlinear electromagnetic field effect," *IEEE/ASME Trans. Mechatronics*, vol. 18, no. 3, pp. 1122–1129, Jun. 2013.
[16] W. Sun, Y. Zhang, Y. Huang, H. Gao, and O. Kaynak, "Transient-performance-guaranteed robust adaptive control and its application to precision motion control systems," *IEEE Trans. Ind. Electron.*, vol. 63, no. 10, pp. 6510–6518, Mar. 2016.
[17] Z. Chen, B. Yao, and Q. Wang, "μ-synthesis-based adaptive robust control of linear motor driven stages with high-frequency dynamics: A case study," *IEEE/ASME Trans. Mechatronics*, vol. 20, no. 3, pp. 1482–1490, Jun. 2015.
[18] J. Yao, Z. Jiao, and D. Ma, "A practical nonlinear adaptive control of hydraulic servomechanisms with periodic-like disturbances," *IEEE/ASME Trans. Mechatronics*, vol. 20, no. 6, pp. 2752–2760, Dec. 2015.
[19] C. Kaddissi, J.-P. Kenné, and M. Saad, "Indirect adaptive control of an electrohydraulic servo system based on nonlinear backstepping," *IEEE/ASME Trans. Mechatronics*, vol. 16, no. 6, pp. 1171–1177, Dec. 2011.
[20] J. Yao, W. Deng, and Z. Jiao, "Adaptive control of hydraulic actuators with LuGre model-based friction compensation," *IEEE Trans. Ind. Electron.*, vol. 62, no. 10, pp. 6469–6477, Oct. 2015.
[21] K. Guo, J. Wei, J. Fang, R. Feng, and X. Wang, "Position tracking control of electro-hydraulic single-rod actuator based on an extended disturbance observer," *Mechatronics*, vol. 27, pp. 47–56, Apr. 2015.
[22] F. Bu and B. Yao, "Adaptive robust precision motion control of single-rod hydraulic actuators with time-varying unknown inertia: A case study," in *Proc. ASME Int. Mechan. Eng. Congr. Expo.*, 1999, pp. 131–138.
[23] W. Sun, S. Tang, H. Gao, and J. Zhao, "Two time-scale tracking control of nonholonomic wheeled mobile robots," *IEEE Trans. Control Syst. Technol.*, vol. 24, no. 6, pp. 2059–2069, Nov. 2016.
[24] B. Helian, Z. Chen, B. Yao, Y. Yan, and C. Lee, "Adaptive robust control of a pump control hydraulic system," in *Proc. ASME Dyn. Syst. Control Conf.*, Oct. 2017, p. V001T15A004, paper DSCC2017-5076.
[25] C. Li, Z. Chen, and B. Yao, "Adaptive robust synchronization control of a dual-linear-motor-driven gantry with rotational dynamics and accurate online parameter estimation," *IEEE Trans. Ind. Informat.*, to be published, doi: 10.1109/TII.2017.2773472.
[26] H. E. Merritt, *Hydraulic Control Systems*. New York, NY, USA: Wiley, 1967.
[27] Y. Wang, X. Gao, and X. Zhang, "Static steering resisting moment of tire for heavy multi-axle steering vehicle," *Trans. Chin. Soc. Agricult. Eng.*, vol. 26, no. 10, pp. 146–150, Oct. 2010.
[28] Y. Zhuang and K. Guo, "Tire spot turn model based on LuGre model," *Automobile Technol.*, vol. 2, no. 7, pp. 001–003, Jun. 2008.
[29] H. B. Pacejka, *Tire and Vehicle Dynamics*. London, U.K.: Butterworth, 2002.
[30] M. Yuan, Z. Chen, B. Yao, and X. Zhu, "Time optimal contouring control of industrial biaxial gantry: A highly efficient analytical solution of trajectory planning," *IEEE/ASME Trans. Mechatronics*, vol. 22, no. 1, pp. 247–257, Feb. 2017.

HENG DU received the B.S. degree from Tongji University, China, in 2006, and the Ph.D. degree from Zhejiang University, China, in 2011. Since 2012, he has been with the School of Mechanical Engineering and Automation, Fuzhou University, China, where he is currently an Associate Professor. His current research interests include the theory and application of electro-hydraulic control, multi-axle steering control, and hydraulic press.

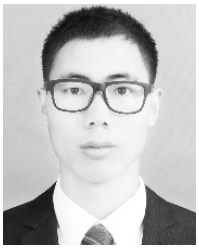

ZHONGBAO WANG received the B.Tech. degree from Fuzhou University, Fuzhou, China, in 2016, where he is currently pursuing the master's degree with the School of Mechanical Engineering and Automation. His current research interests include the nonlinear servo control of mechatronic systems.

YAXIONG WANG (S'13–M'16) received the B.Eng. degree in mechanical engineering from the Chongqing University of Technology, Chongqing, China, in 2010, and the M.Eng. and Ph.D. degrees in mechanical engineering from Chonnam National University, Gwangju, South Korea, in 2012 and 2015, respectively. Then, he was a Postdoctoral Research Associate in the field of fuel cell hybrid vehicles in Chonnam National University. He is currently with the School of Mechanical Engineering and Automation, Fuzhou University, Fuzhou, China. His research interests include PEM fuel cell modeling, control and power optimization, and hybrid renewable power systems energy management.

Dr. Wang was a recipient of the Chinese Government Award for Outstanding Self-Financed Student Abroad. He received the Best Paper Award from Chonnam National University in 2014 and 2015.

HUI HUANG received the B.Sc. and M.Sc. degrees from the School of Mechanical Engineering and Automation, Fuzhou University, in 2009 and 2012, respectively, where he is currently pursuing the Ph.D. degree. He is an Experimentalist with Fuzhou University. His main research interests include hydraulic transmission and control, noise and vibration control, and testing and measurement techniques.